Published in final edited form as:
Biomaterials. 2014 August ; 35(25): 6750–6757. doi:10.1016/j.biomaterials.2014.04.097.

The effects of confinement on neuronalgrowth cone morphology and velocity

Michael S. Smirnov[1,2], **Katelyn A. Cabral**[3], **Herbert M. Geller**[3,*], and **Jeffrey S. Urbach**[2,*]

[1]Interdisciplinary Program in Neuroscience, Georgetown University, Washington DC 20057

[2]Department of Physics, Georgetown University, Washington DC 20057

[3]Developmental Neurobiology Section, Cell Biology and Physiology Center, National Heart, Lung, and Blood Institute, National Institutes of Health, Bethesda, Maryland 20892

Abstract

Optimizing growth cone guidance through the use of patterned substrates is important for designing regenerative substrates to aid in recovery from neuronal injury. Using laser ablation, we designed micron-scale patterns capable of confining dissociated mouse cerebellar granule neuron growth cones to channels of different widths ranging from 1.5 to 12 μm. Growth cone dynamics in these channels were observed using time lapse microscopy. Growth cone area was decreased in channels between 1.5 and 6 μm as compared to that in 12 μm and unpatterned substrates. Growth cone aspect ratio was also affected as narrower channels forced growth cones into a narrow, elongated shape. There was no difference in the overall rate of growth cone advance in uniform channels between 1.5 and 12 μm as compared to growth on unpatterned substrates. The percentage of time growth cones advanced, paused, and retracted was also similar. However, growth cones did respond to changes in confinement: growth cones in narrow lanes rapidly sped up when encountering a wide region and then slowed down as they entered another narrow region. Our results suggest that the rate of neurite extension is not affected by the degree of confinement, but does respond to changes in confinement.

Keywords

Neural cell; polyvinylalcohol; nerve regeneration; laminin; laser ablation

1. Introduction

Strategies for promoting regeneration following injury to the mammalian central nervous system generally incorporate the use of implantable biomaterials to guide neurons [1–4],

Corresponding Author: Jeffrey Urbach, Department of Physics, 320 Regents Hall, Georgetown University, Washington DC 20057, urbach@physics.georgetown.edu, Fax #: (202) 687-2087.
*H.M.G. and J.S.U contributed equally to this work

with extensive research focusing on the design of various topographic and structural patterns in order to direct neuronal outgrowth [5]. Directed neurite outgrowth has been mainly achieved by patterning surfaces with aligned linear features. In addition, the rate of neurite outgrowth on these patterns can be modulated by altering specific structural parameters of the substrate. For example, dorsal root ganglia (DRG) neurons have been shown to extend farther on protein-coated fibers of smaller diameter [6]. DRGs extending along printed channels of laminin, a known permissive substrate, have also shown a preference for certain channel widths [7,8]. The mechanisms underlying these responses to substrate features are not known.

The growth cone is the structure responsible for integrating chemical and structural signals from the extracellular matrix and controlling neurite extension. Growth cones alter their size as well as rate of movement as a response to pattern dimensions [7,9,10]. However, a detailed understanding of these responses is lacking. We employed a laser ablation technique [11] to fabricate a model system of laminin-coated channels for guiding neurons, allowing us to achieve the micron-scale resolution necessary to alter growth cone morphology. Furthermore, we used dissociated cerebellar granule neurons (CGNs) to better identify isolated effects of growth cone size. The objective of our study was to use high-resolution, time-lapse microscopy on live cells extending on our fabricated patterns to evaluate the relationships between substrate structure and growth cone size, shape, and rate of extension.

2. Materials and Methods

2.1 Glass-bottom dish preparation

Dishes were prepared according to a previously published protocol [11]. Briefly, glass-bottom (MatTek) dishes were washed with 50% HNO_3, treated with 200 mM NaOH, rinsed with H_2O, and silanized using 1% triethoxysilylbutraldehyde (Gelest) in ethanol. Surfaces were washed with ethanol and H_2O and allowed to cure for 3 hours at 65°C. A 5.6% PVA solution was prepared by dissolving PVA (molecular weight ≈ 98,000; 98% hydrolyzed; Sigma-Aldrich) in H_2O at 90°C and filtered through a 0.2 μm filter. 2N HCl was added to the filtered PVA at a 1:8 ratio. The mixture was spin-coated onto the silanized glass-bottom dishes at 7000RPM for 45s and the dishes were stored at 4°C.

2.2 Photoablation

A Leica SP5 Multi-Photon (dual beam with OPO)/Confocal Microscope was used for photoablation. ROIs were generated using Leica operating software. A 63x NA 1.4 oil immersion objective was used during ablation. Digital zoom was set to 4× in order to decrease amount of z-tilt in the field of view. Autofocus was performed using reflectance from a low power 633nm laser. Ablation was achieved via a two-photon laser at 800nm and ≈ 35% power, scanning at 100Hz at a 512×512 resolution. These settings allowed us to burn away PVA but prevent scorching of the glass surface. Leica MatrixScreener software was used to automate the process in order to create consistent, tiled patterns. To prevent autofluorescence, dishes were quenched for 8 minutes with 2 ml of 0.5% $NaBH_4$ in 200 mM

Ethanolamine buffer (200 mM $EtOHNH_3$, 100 mM NaH_2PO_4, pH 8.0) and then washed 3x with PBS.

2.3 Laminin labeling and attachment

Laminin was conjugated with Alexa Fluor-488 dye (Life Technologies) using supplied protocols. Fluorescently labeled laminin was diluted to 25 μg/ml in PBS with 0.1% Pluronic F-127 (Life Technologies) and added to coverslips for 30min at room temp. Dishes were washed 3x with PBS and kept in PBS until use.

2.4 Atomic force microscopy (AFM) imaging

Topographic images of the ablated regions were acquired with a Solver Next (NT-MDT) scanning probe microscope operating in oscillating mode.

2.5 Cell culture

Cultures of dissociated mouse CGNs were prepared from postnatal 5-day-old C57BL/6 mice as described previously [12]. Dissociated cells plated on laminin/coated patterns and 2D unpatterned laminin-coated glass dishes in Neurobasal-A medium containing B27 (1 : 50, v/v) supplement, glutaMAX (1 : 100, v/v, Life Technologies), Pen/Strep, and 25 mM KCl.

2.6 Scanning electron microscopy (SEM) preparation and imaging

Coverslip cultures were fixed in 2.5% glutaraldehyde, 1% paraformaldehyde, 0.12 M sodium cacodylate buffer, pH 7.3, postfixed with 1% OsO4 in the same buffer, dehydrated in an ethanol series and critical point dried out of CO_2 in a Samdri-795 critical point dryer (Tousimis Research Corp, Rockville MD). The dried coverslip cultures were coated with 5nm of gold in an EMS 575-X sputter coater (Electron Microscopy Sciences, Hatfield PA) and imaged with a Hitachi S-3400 N1 scanning electron microscope (Hitachi High Technologies America, Inc., Pleasanton CA).

2.7 Time-lapse microscopy

Phase contrast images were obtained using a Nikon Eclipse TE2000-E inverted microscope equipped with a 37°C and 5% CO_2 incubation chamber, 63x oil objective, and a motorized stage (Prior Scientific). Metamorph software (Molecular Devices) with the multidimensional acquisition plugin was used to capture images and control all hardware. Images were acquired using a 63x oil objective and digital camera (Hamamatsu Photonics). Regular time-lapse imaging was performed in ~20 locations at 5min intervals over two 24-hour periods, while high time-resolution imaging was performed in one location at 5s intervals. Laminin fluorescence was detected using epifluorescence illumination with a mercury lamp and a 488 nm filter cube.

2.8 Image processing and analysis

Image processing was performed using ImageJ [13]. Image stacks were imported and drift-stabilized using the Template Matching plugin. The MtrackJ plugin was used to track growth cone position, while area and aspect ratio (calculated as a ratio between major and

minor axes) were measured by manually tracing each growth cones in each frame. Data analysis was completed using Matlab 2013a (MathWorks).

103 growth cones in were measured on uniform channels and in 2D. The wrist of the growth cone was used as the coordinate for growth cone position. Directionality was determined by setting a reference point at the very beginning of each the channel. For unpatterned 2D controls, the reference point was the first position in frame. Movement towards and away from the reference resulted in a negative and positive velocity, respectively. Error due to turning was negligible in the channels since there was no sideways movement without significant forward or backward displacement. Significant turning was noted and manually corrected for in control growth cones. Average velocity for each axon was calculated as a total displacement between the first and last recorded position divided by elapsed time, and In-group velocities were analyzed for average and standard error.

Area and aspect ratio measured in each frame were first averaged for each individual growth cone. These values were then averaged between all growth cones in each group to avoid bias due to varying sample size. Cumulative probability histograms were plotted using raw instantaneous area measurements.

Instantaneous velocities at each timepoint were calculated as a change in position along the axis of the channel from the previous frame to the following frame divided by time. Growth cones moving at a rate higher than 0.2 μm/min for at least three consecutive frames (15 min) were considered advancing, while velocities above 0.2 μm/min for fewer than three frames and velocities between 0.2 μm/min and −0.2 μm/min were considered paused. Growth cones with velocities less than −0.2 μm/min were considered to be retracting.

33 growth cones were measured on patterns of channels interspersed with circular nodes. Instantaneous velocity was calculated as a displacement along the axis of the channel of growth cones in each consecutive frame divided by time between frames. Directionality was again determined using a reference point. Growth cone position reflects distance to the closest node center. Average velocities and standard errors were calculated for each position. A moving average function (bin=4) was used to smooth velocity data before plotting. Growth cone areas were also grouped in 1 μm bins and averaged for each position.

2.9 Statistics

Statistical analysis was performed in MATLAB with a multiple comparison test using a one-way ANOVA. Results were considered statistically significant if $p < 0.05$.

3. Results

To examine growth cone responses to precisely defined μm-scale features, we used ROI-guided two-photon laser ablation to remove polyvinyl alcohol (PVA), a hydrophilic polymer resistant to protein and cell adhesion, from glass-bottom dishes (Fig. 1A). This resulted in grooves of exposed glass surrounded by 100 nm-high walls of PVA (Fig. S1); the scale of pattern features was chosen to best approximate the range of CGN growth cone sizes *in vitro*. The substrate was then incubated with 25 μg/ml laminin to support adhesion and

growth. Laminin only adhered to glass exposed by the photoablation process, and its concentration remained consistent throughout the pattern, as verified with fluorescence imaging of Alexa Fluor® 488 labeled laminin (Fig. 1B).

3.1 Effects of confinement on growth cone morphology

In order to evaluate the effect of varying degrees of confinement on growth cone size, we created patterns consisting of parallel channels 1.5 μm, 3 μm, 6 μm, and 12 μm wide. Postnatal day 5 CGNs were plated and allowed to settle for 24h to ensure proper adhesion to the patterned substrate. Cells were then imaged using time-lapse phase contrast microscopy for 48h (Movie 1). CGNs consistently extended their neurites along the laminin-coated patterns, and neurites were never observed to extend onto unablated regions. While growth cone filopodia and lamellipodia often explored immediately outside and above the confined pattern, growth cones themselves were confined to their respective channels, with growth cones appearing larger in wider channels (Fig. 2A).

SEM examination revealed that channel width also affected the three-dimensional shape of the growth cones: narrower channels tended to produce growth cones with a thick, tube-like appearance and often vertically-oriented filopodia, while wider channels tended to produce flatter growth cones with more lamellipodia (Fig. 2B).

The area of each growth cone in each frame of the time lapse video was measured by tracing the outline of the growth cone (Fig. 2A). We found a significant effect of confinement on growth cone area: growth cones were largest on 12 μm channels and unpatterned, laminin-coated glass, and significantly smaller on the narrower channels. However, we found no significant difference in area between 1.5 μm, 3 μm, and 6 μm channels (Fig. 2C).

We then plotted the cumulative distributions of individual area measurements of all growth cones at all times for each lane width (Fig. 2E). Growth cone area in all channels had a wide distribution, ranging from 2–130 μm^2, with most falling between 5–75 μm^2. All but the 12 μm channels, including the unpatterned 2D group, have a large portion of small growth cone areas. In contrast, there was an increased proportion of larger growth cone areas recorded in 12 μm channels, although these values were recorded from a few growth cones and therefore are not significantly reflected in the averages in Fig. 2C.

Growth cone aspect ratio was computed using the major and minor axis calculated from each trace. Average aspect ratio was significantly increased in 1.5–6 μm channels compared to 12 μm and unpatterned surfaces, as confinement results in a narrowing and elongation of growth cones (Fig. 2D).

3.2 Effects of confinement on growth cone velocity

To examine how confinement influences extension rate, we compared growth cone velocities in each channel. For a consistent measure of location, growth cone position was measured at the wrist (Fig. 3A), the least dynamic point in the structure. The average velocity for each growth cone was calculated as the total displacement between the positions observed in the first and last frame divided by the elapsed time. Growth cone velocity ranged from −0.08 to 1.6 μm/min, and velocities were relatively tightly grouped in narrow

channels, but had a wider distribution in the 12 μm channel (Fig. 3B). When calculated from average displacement between consecutive frames instead of total displacement, velocities had a wider distribution in the 2D condition (Fig. 3D). However, we found that average velocity was independent of channel width (Fig. 3C). Therefore, altering growth cone area through confinement does not in itself alter average velocity.

Although overall velocities were not significantly different, the possibility remained that channel width could influence growth cone dynamics. We therefore examined the distribution of growth cone advances, pauses, and retractions in each channel (Fig. 4A). Growth cones in 1.5 μm channels spent significantly more time pausing than growth cones on unpatterned surfaces. An opposite trend was observed for the percentage of time advancing, though this did not reach statistical significance (Fig. 4B). Furthermore, growth cones on unpatterned substrates spent more time retracting than growth cones on 12 μm channels.

3.3 Effects of alternating confinement on growth cones

Growth cones of retinal ganglion axons alter both their velocity and shape when then enter the optic chiasm [14]. We therefore sought to evaluate whether increased confinement would alter growth cone velocity and shape. We plated CGNs on patterns with 1.5 μm channels interspersed with repeating circular nodes 10 μm in diameter at 60 μm intervals, and imaged growth cones over time as they traversed the patterns. Growth cones in the 1.5 μm-wide region displayed similar behavior to those found in uniform channels: advancing, retracting, and pausing in a seemingly unpredictable manner. However, once growth cones encountered a node, they rapidly accelerated into the node and spread out their filopodia and lamellipodia. Once inside the node, growth cones slowed down and spent time exploring the edges of the node, and ultimately proceeded into the continuing channel (Movie 2).

For each growth cone in every frame, position was recorded relative to the center of the nearest node. A histogram of the data reveals fewer growth cones in the location approaching the node (Fig. 5A). In contrast, growth cones are more frequently found inside and following the node. Average instantaneous velocity at each position relative to the node was calculated using individual growth cone displacements between consecutive frames. Growth cones displayed up to a three-fold increase in velocity as they are approaching and entering the node: between −15 μm and −10 μm from node center, average velocity was 0.34 ± 0.09 μm/min (Fig. 5B). Once inside the node, growth cone velocity dropped significantly: between −5 μm and 5 μm from the center of the node, average growth cone velocity was 0.06 ± 0.01 μm/min. After growth cones left the node, their velocity increased to 0.13 ± 0.01 μm/min. This velocity is slightly smaller than in channels with a consistent 1.5 μm width, where growth cones traveled at an average of 0.17 ± 0.03 μm/min. These changes in velocity were accompanied by substantial changes in growth cone area. Preceding and following the node, area hovered around 20–25 μm^2, similar to that found in the uniform 1.5 μm channels (Figs. 5C, 3C). However, as growth cones entered and explored the node, their area increased to a range of 30–40 μm^2. Thus, once inside the node, changes in growth cone area and velocity are inversely correlated.

4. Discussion

With the use of micron-scale laser patterning, we engineered substrates that confined CGN growth cones to narrow channels of defined width, allowing high-resolution time-lapse imaging to evaluate the growth and morphology of growth cones over long periods of time as they traversed these channels. Confining growth cones to uniform channels of different widths influences their morphology but not their velocity, suggesting that altering growth cone shape alone does not alter velocity. However, we found that growth cones did respond to changes in channel width: growth cones sped up and then slowed down as they entered nodes interspersing narrow channels. Growth cone morphology was also responsive to decreased confinement, as growth cones rapidly enlarged upon entering a node. Thus, in confinement, growth cone motility appears to be responsive to changes in the environment, but not to the confinement process itself.

We employed a recently established laser ablation technique [11] to create micron-scale adhesive channels capable of confining neuronal growth cones. This technique generates sub-micron resolution laminin-coated patterns surrounded by a completely non-adhesive region of PVA. The ability to produce these patterns in glass-bottom dishes allowed us to perform high-resolution time-lapse imaging on live neurons. Currently, the most common technique for producing narrow lanes with adhesive ligands is microcontact printing, where a polydimethylsiloxane (PDMS) stamp is created using lithographic techniques [7,15,16], yet this method has certain shortcomings. Microcontact printing requires a relatively adhesive surface for proteins to attach, often resulting in some nonspecific cell adhesion. Poly-L-Lysine, for example, is often used as an adhesive substrate, and thus prevents the establishment of a true inhibitory barrier outside of the pattern. Furthermore, protein concentration on stamped surfaces can be quite variable [17]. A patterning approach which combats these issues is microfluidics [18,19], but patterns with features smaller than 10μm are difficult to make, and either require very advanced equipment or are prohibitively expensive. One limitation of our technique was the considerable amount of time required to prepare a single patterned dish (~3 hours per 2mm^2 pattern), although ablating dishes individually allows for fine-tune pattern features between experiments.

We evaluated the outgrowth of isolated CGNs in laminin-coated channels whose width was varied between 1.5 and 12 μm. As previously observed for other cell types [20], we found that laminin patterns were very effective in confining and promoting CGN neurite outgrowth, with very few growth cones ever leaving the channels. Average growth cone velocity in uniform channels did not depend on channel width and did not differ significantly from growth rates on a uniform substrate of laminin. Tai and Buettner [7], on the other hand, found that DRGs on an unpatterned surface extend faster than those in confined lanes. In contrast to those results, Song and Uhrich [8] found that DRG neurites extend fastest in laminin stripes as compared to an unpatterned surface, but their patterns were not meant to fully confine neurons, and therefore show a significant amount of fasciculation and interaction between axons. We found CGNs to be ideal for growth cone isolation, since DRG cultures are often confounded by effects of clustering due to a high amount of branching and are very heterogeneous. Our results with CGNs complement

previous studies in that our lane widths are capable of reducing growth cone size, allowing us to isolate the influence of growth cone size on extension rate.

Time-lapse imaging revealed that growth cones did not grow steadily: they would pause, advance, and retract. Neurons in 2D environments also exhibit similar behavior [21]. *In vivo*, pausing tends to be associated with decision regions and changes in directionality [22,23]. Consequently, one could assume that on confined, linear substrates where growth cones lack choice in directionality, pausing would be unnecessary while forward growth would be more consistent. It is therefore curious that varying channel width proved to have little effect on the percentages of time of time spent pausing or advancing. Furthermore, growth cones on 2D surfaces actually spent relatively less time pausing than those on 1.5 μm channels. Weigel et al. [24] found that chick spinal cord neurons grown between elevated ridges exhibited a similar behavior: the percentage of time where velocity was positive remained between 70 and 80% regardless of the inter-ridge distance which growth cones occupied. Average positive and negative velocities were also fairly consistent at about 85 and −70 μm/h, respectively. The same methods of analysis applied to our data show that positive velocities were recorded between 60 and 65% of the time, while average positive and negative velocities had a much lower magnitude at 23 and −20 μm/h. These differences in velocity can likely be attributed to cell type and substrate composition.

Growth cone area and aspect ratio were found to vary with channel width. CGN growth cones on wide lanes and 2D unpatterned surfaces were on average 1.5 – 2 times larger than those on narrower lanes. Two groups reported similar alterations in DRGs: as compared to growth cones on unpatterned surfaces, growth cone size was reduced in lanes narrower than 20 μm [9] and increased in lanes wider than 20μm [7]. Under some conditions, axons outgrowth is edge-guided [25], and it is possible that wider channels drive growth cones to enlarge in order to contact with both edges at once. Although average growth cone area was not statistically different between 12 μm and 2D groups, the distribution of all growth cones at all times showed that some growth cones in 12 μm channels were noticeably larger, suggesting that this phenomenon may be present in our system as well. The wide area distributions in each group are likely explained by growth cones' phasic process of spreading out and contracting their filopodia and lamellipodia [26]. Previous studies have also shown that growth cone height decreases as a result of spreading out on laminin lanes [27]. While we were unable to quantify growth cone volume, growth cones in wider lanes appeared flatter when examined under SEM, suggesting a 3D cytoskeletal rearrangement in response to confinement.

Growth cone area was also found to change as neurons encountered increases and decreases in channel width. As they entered a node, growth cones both grew larger and slowed down. Féréol et al. [28] observed a similar behavior in DRG growth cones which spread out and paused as they entered a laminin spot, yet remained highly dynamic while supposedly searching for their next target. After exiting a node, growth cone area again decreased inside confined channels. This is reminiscent of the behavior of retinal ganglion cells: growth cones tend to be small and streamlined in the optic nerve, but as they reach the optic chiasm, they often become larger and tend to pause [14,29]. Similarly, Liu et al. [10] found that hippocampal growth cones increased in size when leaving a 5 μm lane and entering an open,

2D region, at which point they were more likely to branch. It is worth noting, however, that the growth cone area measured in the nodes was equal to that of growth cones continuously confined to channels of the width of the node, suggesting that the spreading of the growth cone is not dependent on the previous state of confinement.

A lack of influence by substrate confinement, and thus growth cone area, on extension rate may seem puzzling due to the growth cone's established role as the primary mechanistic center in axon extension. The most parsimonious explanation is that there exists a feedback mechanism that maintains the overall elongation rate. There are a wide range of factors that can modulate axon growth rate, for example laminin concentration [30,31]. While larger growth cones might sense more laminin, smaller growth cones might compensate with an alteration in integrin expression to sustain a necessary growth rate, as neurons have been shown to vary their expression levels of integrins based on laminin concentration in the substrate [32]. A feedback mechanism could also operate through the rate of tubulin polymerization or the organization of microtubules in the neurite shaft, which is tightly regulated, in part through interaction with MAPs [33].

That there are actually differences in the growth cones in different width lanes is evidenced by the "jumping" behavior as growth cones encounter a node, suggesting that a sudden change in substrate width disrupts an established steady state equilibrium, resulting in unusually quick growth as more laminin area is encountered in the node. This phenomenon is similar to the rapid movement of DRG growth cones growing on fibronectin once their filopodia touch laminin [34]. There are several potential explanations for this behavior. The 'jump' could be a response to an increased amount of laminin ahead of the growth cone, since receptors on growth cone filopodia influence neurite outgrowth when contacting patterned ECM substrates [35,36]. The high laminin availability does not produce higher growth rates in axons that are continually confined to the wider lanes, presumably because they have already adapted to the higher laminin availability. Integrins on filopodia couple with laminin to form highly dynamic point contacts [37] which are also involved in growth cone guidance [38,39]. Growth cones likely form more point contacts in the node, and are therefore may be pulled forward as a result of the increase in force that would arise from a transition to a larger area of traction stresses, like those observed in DRG growth cones on uniform 2D substrates [40]. Further studies are clearly necessary to identify those factors responsible for establishing this equilibrium.

5. Conclusions

Many different patterning techniques have been used to evaluate growth cone dynamics in vitro. Laser-guided patterning has the advantage of producing consistent, micron-scale patterns that can be easily modified to test specific hypotheses. While it has been established that substrate feature size is capable of controlling neuronal outgrowth rates, we have shown that altering growth cone size, per se, will not modulate growth velocity. However, we demonstrated that growth cones do respond to changes in their environment with a change in size and axonal extension rate. In decision regions, this change in growth cone size and velocity has been linked to a change in sensitivity to guidance cues, and we propose that our assay can provide a systematic test of this hypothesis.

Supplementary Material

Refer to Web version on PubMed Central for supplementary material.

Acknowledgments

Special thanks to Dr. Andrew Doyle as well as the NHLBI Light Microscopy Core for their help with the photoablation process and to the NHLBI EM Core for their help in collecting SEM images. Funding was provided by NIH grant 1R01NS064250 to J.S.U. and the NHLBI Intramural Research Program (H.M.G).

References

1. Geller HM, Fawcett JW. Building a bridge: engineering spinal cord repair. Exp Neurol. 2002; 174:125–36. [PubMed: 11922655]
2. Norman LL, Stroka K, Aranda-Espinoza H. Guiding axons in the central nervous system: a tissue engineering approach. Tissue Eng Part B Rev. 2009; 15:291–305. [PubMed: 19435403]
3. Biazar E, Khorasani MT, Montazeri N, Pourshamsian K, Daliri M, Rezaei M, et al. Types of neural guides and using nanotechnology for peripheral nerve reconstruction. Int J Nanomedicine. 2010; 5:839–52. [PubMed: 21042546]
4. Straley KS, Foo CWP, Heilshorn SC. Biomaterial design strategies for the treatment of spinal cord injuries. J Neurotrauma. 2010; 27:1–19. [PubMed: 19698073]
5. Hoffman-Kim D, Mitchel JA, Bellamkonda RV. Topography, cell response, and nerve regeneration. Annu Rev Biomed Eng. 2010; 12:203–31. [PubMed: 20438370]
6. Xuejun W, Tresco PA. Effect of filament diameter and extracellular matrix molecule precoating on neurite outgrowth and Schwann cell behavior on multifilament entubulation bridging device in vitro. J Biomed Mater Res A. 2006; 76:626–37. [PubMed: 16287096]
7. Tai HC, Buettner HM. Neurite outgrowth and growth cone morphology on micropatterned surfaces. Biotechnol Prog. 1998; 14:364–70. [PubMed: 9622516]
8. Song M, Uhrich KE. Optimal micropattern dimensions enhance neurite outgrowth rates, lengths, and orientations. Ann Biomed Eng. 2007; 35:1812–20. [PubMed: 17616821]
9. Clark P, Britland S, Connolly P. Growth cone guidance and neuron morphology on micropatterned laminin surfaces. J Cell Sci. 1993; 105(Pt 1):203–12. [PubMed: 8360274]
10. Liu W, Xing S, Yuan B, Zheng W, Jiang X. Change of laminin density stimulates axon branching via growth cone myosin II-mediated adhesion. Integr Biol (Camb). 2013; 5:1244–52. [PubMed: 23959160]
11. Doyle AD. Generation of micropatterned substrates using micro photopatterning. Curr Protoc Cell Biol. 2009; 10:10.15.
12. Wang H, Katagiri Y, McCann TE, Unsworth E, Goldsmith P, Yu Z-X, et al. Chondroitin-4-sulfation negatively regulates axonal guidance and growth. J Cell Sci. 2008; 121:3083–91. [PubMed: 18768934]
13. Schneider CA, Rasband WS, Eliceiri KW. NIH Image to ImageJ: 25 years of image analysis. Nat Methods. 2012; 9:671–5. [PubMed: 22930834]
14. Mason, Ca; Wang, LC. Growth cone form is behavior-specific and, consequently, position-specific along the retinal axon pathway. J Neurosci. 1997; 17:1086–100. [PubMed: 8994063]
15. Ruiz A, Buzanska L, Gilliland D, Rauscher H, Sirghi L, Sobanski T, et al. Micro-stamped surfaces for the patterned growth of neural stem cells. Biomaterials. 2008; 29:4766–74. [PubMed: 18819707]
16. Théry M, Piel M. Adhesive micropatterns for cells: a microcontact printing protocol. Cold Spring Harb Protoc. 2009 pdb.prot5255.
17. Whitesides GM, Ostuni E, Takayama S, Jiang X, Ingber DE. Soft lithography in biology and biochemistry. Annu Rev Biomed Eng. 2001; 3:335–73. [PubMed: 11447067]

18. Yuan B, Li Y, Wang D, Xie Y, Liu Y, Cui L, et al. A general approach for patterning multiple types of cells using holey PDMS membranes and microfluidic channels. Adv Funct Mater. 2010; 20:3715–20.
19. Kim P, Kwon K, Park M, Lee S, Kim S, Suh K. Soft lithography for microfluidics: a review. 2008; 2:1–11.
20. Hammarback J, McCarthy J, Palm S. Growth cone guidance by substrate-bound laminin pathways is correlated with neuron-to-pathway adhesivity. Dev Biol. 1988; 126:29–39. [PubMed: 3342934]
21. Argiro V, Bunge M, Johnson M. Correlation between growth form and movement and their dependence on neuronal age. J Neurosci. 1984; 4:3051–62. [PubMed: 6502223]
22. Godement P, Wang L-C, Mason CA. Retinal axon divergence in the optic chiasm: dynamics of growth cone behavior at the midline. J Neurosci. 1994; 14:7024–39. [PubMed: 7965096]
23. Skaliora I, Adams R, Blakemore C. Morphology and growth patterns of developing thalamocortical axons. J Neurosci. 2000; 20:3650–62. [PubMed: 10804207]
24. Weigel S, Osterwalder T, Tobler U, Yao L, Wiesli M, Lehnert T, et al. Surface microstructures on planar substrates and textile fibers guide neurite outgrowth: a scaffold solution to push limits of critical nerve defect regeneration? PLoS One. 2012; 7:e50714. [PubMed: 23251379]
25. Xing S, Liu W, Huang Z, Chen L, Sun K, Han D, et al. Development of neurons on micropatterns reveals that growth cone responds to a sharp change of concentration of laminin. Electrophoresis. 2010; 31:3144–51. [PubMed: 20803500]
26. Gallo G, Pollack ED. Cyclic remodelling of growth cone lamellae and the effect of target tissue. Brain Res Dev Brain Res. 1995; 85:140–5.
27. Messa M, Canale C, Marconi E, Cingolani R, Salerno M, Benfenati F. Growth cone 3-D morphology is modified by distinct micropatterned adhesion substrates. IEEE Trans Nanobioscience. 2009; 8:161–8. [PubMed: 19366649]
28. Féréol S, Fodil R, Barnat M, Georget V, Milbreta U, Nothias F. Micropatterned ECM substrates reveal complementary contribution of low and high affinity ligands to neurite outgrowth. Cytoskeleton (Hoboken). 2011; 68:373–88. [PubMed: 21692191]
29. Bovolenta P, Mason C. Growth cone morphology varies with position in the developing mouse visual pathway from retina to first targets. J Neurosci. 1987; 7:1447–60. [PubMed: 3572487]
30. Marquardt L, Willits RK. Neurite growth in PEG gels: effect of mechanical stiffness and laminin concentration. J Biomed Mater Res A. 2011; 98:1–6. [PubMed: 21538826]
31. Swindle-Reilly KE, Papke JB, Kutosky HP, Throm A, Hammer Ja, Harkins AB, et al. The impact of laminin on 3D neurite extension in collagen gels. J Neural Eng. 2012; 9:046007. [PubMed: 22736189]
32. Condic ML, Letourneau PC. Ligand-induced changes in integrin expression regulate neuronal adhesion and neurite outgrowth. Nature. 1997; 389:852–6. [PubMed: 9349817]
33. Tymanskyj SR, Scales TME, Gordon-Weeks PR. MAP1B enhances microtubule assembly rates and axon extension rates in developing neurons. Mol Cell Neurosci. 2012; 49:110–9. [PubMed: 22033417]
34. Gomez TM, Letourneau PC. Filopodia initiate choices made by sensory neuron growth cones at laminin/fibronetin borders in vitro. 1994:74.
35. Mortimer D, Fothergill T, Pujic Z, Richards LJ, Goodhill GJ. Growth cone chemotaxis. Trends Neurosci. 2008; 31:90–8. [PubMed: 18201774]
36. Geraldo S, Gordon-Weeks PR. Cytoskeletal dynamics in growth-cone steering. J Cell Sci. 2009; 122:3595–604. [PubMed: 19812305]
37. Steketee MB, Tosney KW. Three functionally distinct adhesions in filopodia: shaft adhesions control lamellar extension. J Neurosci. 2002; 22:8071–83. [PubMed: 12223561]
38. Gomez TM, Roche FK, Letourneau PC. Chick sensory neuronal growth cones distinguish fibronectin from laminin by making substratum contacts that resemble focal contacts. J Neurobiol. 1996; 29:18–34. [PubMed: 8748369]
39. Myers JP, Gomez TM. Focal adhesion kinase promotes integrin adhesion dynamics necessary for chemotropic turning of nerve growth cones. J Neurosci. 2011; 31:13585–95. [PubMed: 21940449]

40. Koch D, Rosoff WJ, Jiang J, Geller HM, Urbach JS. Strength in the periphery: growth cone biomechanics and substrate rigidity response in peripheral and central nervous system neurons. Biophys J. 2012; 102:452–60. [PubMed: 22325267]

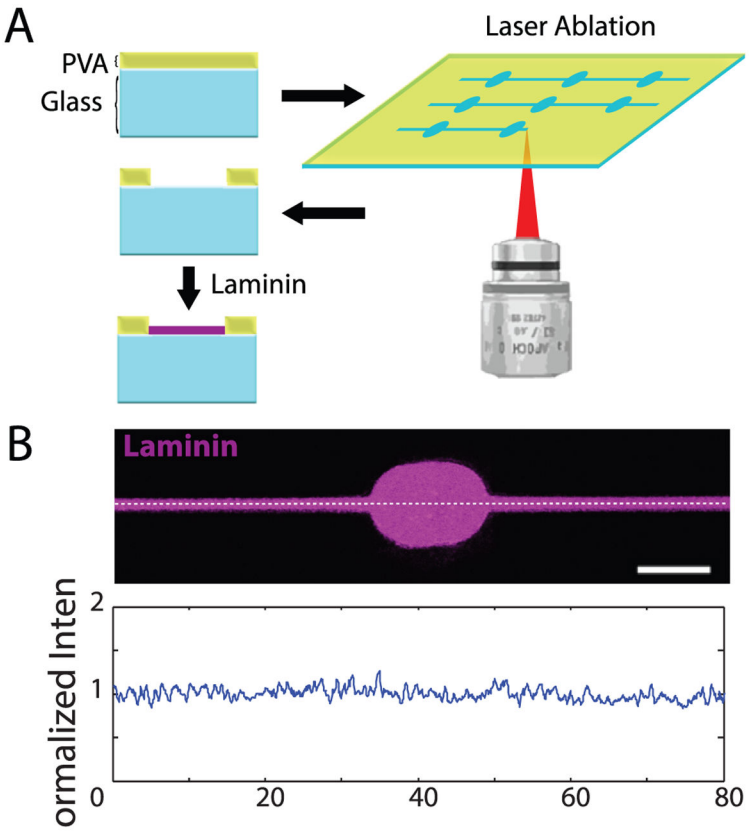

Figure 1.

Generation of laminin-coated patterns using laser photoablation. (A) A thin layer of PVA on top of glass is selectively ablated using repetitive high-power laser scanning in a region of interest. Laminin selectively adheres to glass exposed by the ablation process. (B) AlexaFluor-488 laminin (purple) after adhesion to photoablated dish. Bottom: moving average (bin of 5 pixels) of a fluorescence intensity plot along the white dashed line divided by overall average intensity. Scale bar = 10 μm.

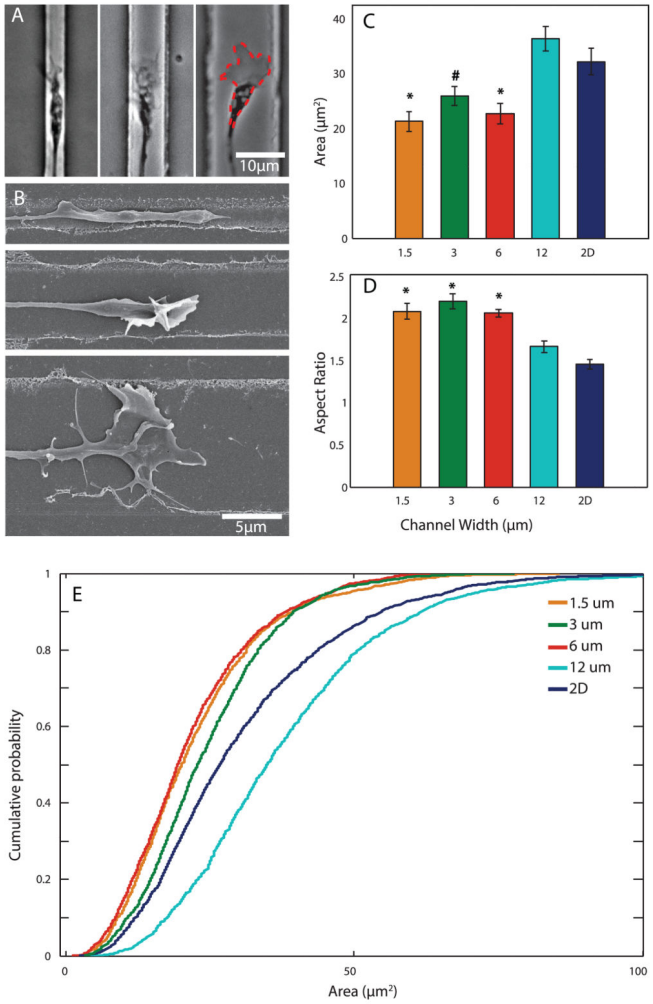

Figure 2.

Channel width controls growth cone morphology. (A) Left to right: representative brightfield images of growth cones in 1.5 μm, 6 μm, and 12 μm channels. Red dashed outline indicates typical area measurement. (B) Representative SEM images of growth cones in different channels. Top to bottom: 1.5 μm, 6 μm, 12 μm channels. (C, D) Average growth cone area and aspect ratio (major/minor axis) in each group. 2D indicates unpatterned substrate. *N*=19, 15, 22, 19, and 28 for 1.5 μm, 3 μm, 6 μm, 12 μm, and 2D, respectively. (E) Cumulative distribution histogram of individual growth cone area measurements. **p*<0.05 when compared to 12 μm and 2D groups. #*p*<0.05 when compared to 2D group.

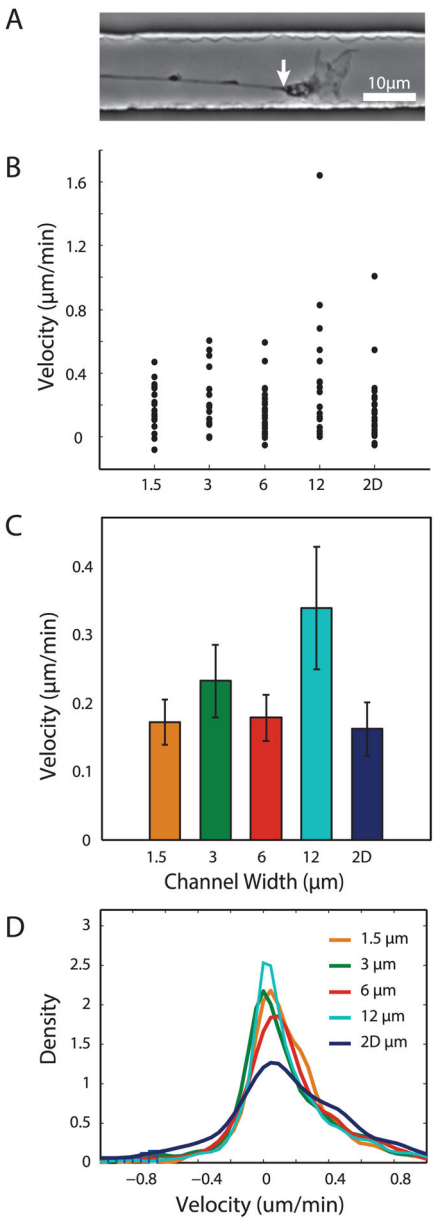

Figure 3.

Growth cone velocity is not affected global variations in channel width. (A) Representative brightfield image indicating wrist (white arrow) of growth cone used as marker for position. (B,C) Distribution and average of growth cone velocities based on total displacement in each group. *N*=19, 15, 22, 19, and 28 for 1.5μm, 3μm, 6μm, 12μm, and 2D, respectively. (D) Smoothed histogram of instantaneous velocities from all growth cone positions.

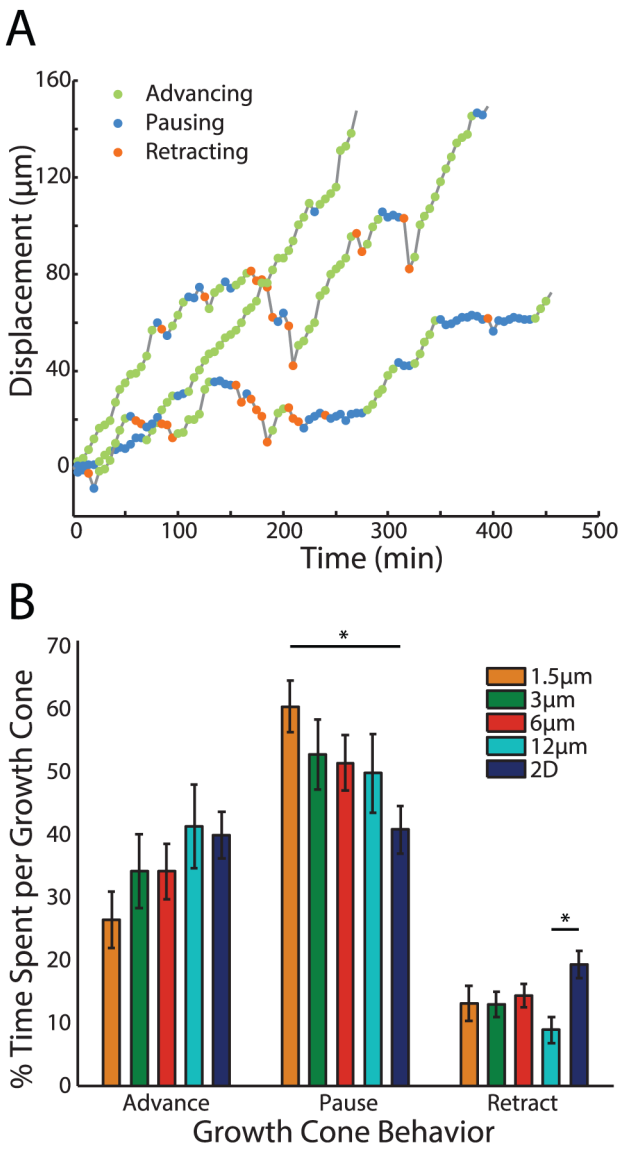

Figure 4.

Growth cone behavior is altered by channel width. (A) One-dimensional displacement over time of a single growth cone extending along a channel. Circles represent categorization of motion at each point based on velocity. (B) Average of percentage of time spent advancing, pausing, and retracting for growth cones in each group. *$p<0.05$.

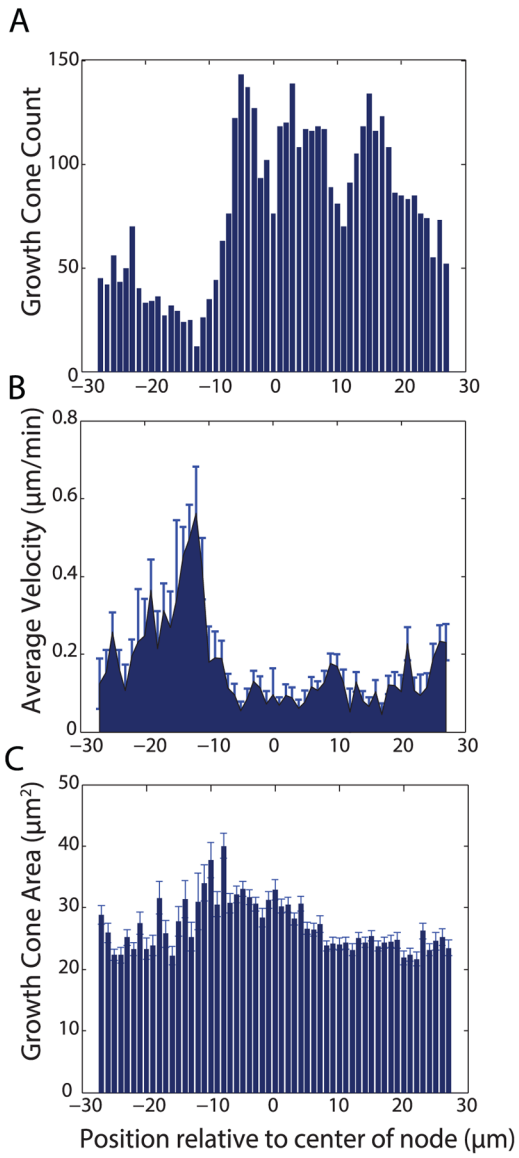

Figure 5.

Growth cones respond to local changes in channel width. (A) Histogram of total recorded growth cone locations in all timeframes and growth cones relative to center of node. (B) Average growth cone velocity at each location relative to center of node (B) Growth cone area averaged at each location measured from center of node. Node is located at −5 to +5 microns